Novel Approach to the Detection of Triacetone Triperoxide (TATP): Its Structure and Its Complexes with Ions

F. Dubnikova,[†] R. Kosloff,[‡] Y. Zeiri,*[,§] and Z. Karpas[§]

Institute of Chemistry, Hebrew University, Jerusalem, Israel, Fritz Haber Center for Molecular Dynamics, Hebrew University, Jerusalem, Israel, and Chemistry Division, Nuclear Research Center, Negev, Beer-Sheva, Israel

Received: November 14, 2001; In Final Form: March 6, 2002

Vapors of chemical substances may be detected with a solid-state sensor coated with a layer that selectively and specifically forms a bond with the vapor, leading to changes in the physicochemical properties of the sensor device. Triacetone triperoxide (TATP) is a homemade explosive that may evade detection by most commonly used detectors but could be detected by a sensor with the proper coating. The conformation and the strength of the bond formed between TATP and several ions—Li^+, Cu^+, Zn^{2+}, Cd^{2+}, In^{3+}, Sb^{3+}, Sc^{3+}, and Ti^{4+}—have been calculated by quantum chemical methods. It was found that of the ions tested in the present work the bonds formed between TATP and Zn^{2+} and In^{3+} were the strongest and the interaction with Sb^{3+}, Sc^{3+}, and Ti^{4+} leads to cleavage of the TATP ring. Thus, in principle, a coating with a suitable ion may serve as the key element for detection of concealed TATP.

Introduction

Among homemade explosives, triacetone triperoxide (TATP) is possibly the most widely used in acts of terror and sabotage in Israel[1] and has been implicated in such acts in the United States[2] and the United Kingdom.[3] It is manufactured by acid catalysis from readily available chemicals (acetone and hydrogen peroxide) that can be purchased on the open market and are virtually impossible to control.[4] Although TATP has been known for several decades,[5] it has been the subject of relatively few publications in the scientific literature.[1,6−8] It was first characterized in a forensic laboratory and positively identified by mass spectrometry less than 20 years ago[6] and further described a few years later.[8] Some of the chemical properties of TATP were recently discussed in a paper dealing with disposing of TATP[9], and its identification in post-explosion debris and residues was presented only this year.[1] Because of its low chemical stability and sensitivity to mechanical shock, TATP is not used in industrial and military applications.[7]

Most modern "plastic explosives" such as cyclotrimethylenetrinitramine (RDX), pentaerythritol (PETN), and their popular composite (Semtex) have extremely low vapor pressures that render their detection by "sniffing" devices very difficult.[10] Thus, the major obstacle in the detection of concealed plastic explosives is that of sampling (i.e., getting enough molecules to the sensor) rather than the lack of sensitivity or ambiguous identification. Most conventional explosives detectors rely on the presence of nitro groups in the explosive molecule to obtain a positive response. TATP, which has a considerable vapor pressure even at ambient temperatures, may be readily sampled and introduced into the detector, but because of the fact that there are no nitro groups in the molecule, detection of concealed TATP presents a serious challenge to counter-terrorism and security forces. The advent of small, portable, solid-state sensors relying on changes in the physical or chemical properties of an array of metal oxide or coated quartz sensors presents new opportunities for detection of explosives such as TATP. These sensors include devices such as quartz microbalances (QMB), surface acoustic waves (SAW), and bulk acoustic waves (BAW), or they rely on the measurement of changes in the conductance of a coating layer.[11] In all cases, the basic requirement is the development of a coating that will selectively and specifically form a bond with the TATP molecules so that the measured property will be related to its concentration in the sampled air.

The novel approach described in the present work draws upon a unique feature of the TATP molecule—its nine-membered ring structure that can form a relatively stable complex with a central moiety to which it then bonds. The concept is analogous to the formation of clatherates or, more specifically, to crown ethers that can selectively bind ionic species from a solution and act as efficient chromatographic resins, as demonstrated in a recent publication.[12] This approach has been theoretically tested with several monovalent, divalent, and trivalent ions as well as with tetravalent Ti^{4+}, which may serve as the active element in the coating layer of a solid-state device. The results of such theoretical calculations at different levels of sophistication are presented in the following sections. The objective of this work is to supply the theoretical basis, derived from rigorous calculations, that may serve as the foundation for a different type of explosives detector and steer the research toward a promising approach.

Method of Calculation

Molecular mechanics force field calculations (MMFF94) using the SPARTAN code (Spartan SGI, version 5.1.3 OpenGL) were used to obtain an approximation of a reliable initial geometry and to determine the most stable conformation of TATP as well as that of some ion−TATP complexes. First, the Zn^{2+} complex with TATP was used to perform a thorough investigation of the lowest-energy geometry using the molecular

* Corresponding author. E-mail: Yehuda@gbumail.bgu.ac.il.
[†] Institute of Chemistry, Hebrew University.
[‡] Fritz Haber Center for Molecular Dynamics, Hebrew University.
[§] Nuclear Research Center.

10.1021/jp014189s CCC: $22.00
Published on Web 04/18/2002

TABLE 1: Binding Energies (kcal/mol) for Ion−TATP and Ion−$(AP)_3$ Complexes

	HF/3-21G+LANL2DZ ECP		HF/3-21G+CRENBL ECP		B3LYP/6-31G**+CRENBL ECP	
ion	without ZPE	with ZPE	without ZPE	with ZPE	without ZPE	with ZPE
Cu^+	68.58	68.70	55.89		58.04	
Li^+	85.60[a]	83.06			68.50[a]	
Cd^{2+}	172.61	171.43	169.84		176.83	
Zn^{2+}	208.33	207.37	194.24		215.21	213.76
In^{3+}	399.19	394.63	379.82		397.67	
Sb^{3+}	394.23	390.43	380.90		559.56[b]	
Sc^{3+}			359.01		638.45[b]	
Ti^{4+}			996.42[b]	995.28[b]	1295.68[b]	

[a] Calculated with a full electron basis set. [b] This value is calculated with respect to the three free acetone peroxide molecules plus the ion.

mechanics code. The results of these calculations were employed as guesses of the initial geometry in Hartree−Fock (HF) calculations. The HF calculations confirmed that the most stable conformations found by the molecular mechanics method were also the most stable at the ab initio level. The most stable conformation was obtained by performing geometry optimization with a number of different initial structures. Calculations were performed for complexes of TATP with the following ions: Li^+, Cu^+, Zn^{2+}, Cd^{2+}, In^{3+}, Sb^{3+}, Sc^{3+}, and Ti^{4+}. The HF method was utilized with a 3-21G basis set for the H, C, and O atoms and a Hay−Wadt LANL2DZ effective core potential (ECP) for all the ions.[13,14] Harmonic vibrational frequencies were evaluated at this level of the theory to confirm that the optimized structure is indeed a local minimum. In addition, the influence of the zero-point energy (ZPE) correction on the calculated binding energies was examined at this level of theory. Because the trivalent ions (In^{3+} and Sb^{3+}) have large electron deficiencies, an additional optimization was performed for their complexes utilizing the Christiansen et al. large orbital basis, small core potential (CRENBL ECP).[14,15] These calculations were carried out starting from the optimal structures obtained from the previous-level calculations (HF with LANLD2DZ ECP). The accuracy of the calculations using effective core potentials was examined by performing a full-electron HF calculation for In^{3+} with a 3-21G basis set to represent the In^{3+} ion. Excellent agreement was found between the results computed with both basis sets.

In the final stage, calculations were carried out with the more sophisticated density functional theory (DFT) with an appropriate basis set. The objective of this last stage was to obtain a higher degree of accuracy in both the geometry and binding energies of the ion−TATP complexes. It should be noted that the complex binding-energy calculation is the key element of the results because it is indicative of the strength by which the TATP molecules attach to the coating layer on the sensing device. The calculations were performed at the B3LYP level (the Becke three-parameter hybrid method[16] with the Lee−Yang−Parr correlation functional approximation[17]). The 6-31G** basis set was used in the description of H, C, and O atoms, and the CRENBL ECP basis was utilized for all of the heavy-metal ions. The DFT approach with the B3LYP approximation has been proven to be quite reliable for descriptions of metal ion−molecule complexes. Some recent examples are associated with complexes involving the Cu^+ ions.[18−20]

Calculations related to the Li^+−TATP complex were performed with the full-electron basis set for Li^+ at both the HF/3-21G and B3LYP/6-31G** levels of theory. This approach was necessary because using the effective core potential in the case of Li^+ results in a calculation with no valence electrons; hence, the total energy of Li^+ becomes zero in such a situation.

In all of the calculations, the optimization was performed without any symmetry restrictions. Both DFT and HF calculations were carried out using the Gaussian 98 program package.[21] The analysis of each orbital population was carried out using the natural bond orbitals (NBO) population analysis,[23] and calculations of atomic charges were performed using both the Mulliken[22] and NBO methods.[23] Both atomic charge and orbital population estimations were carried out for the structures obtained using only the DFT approach.

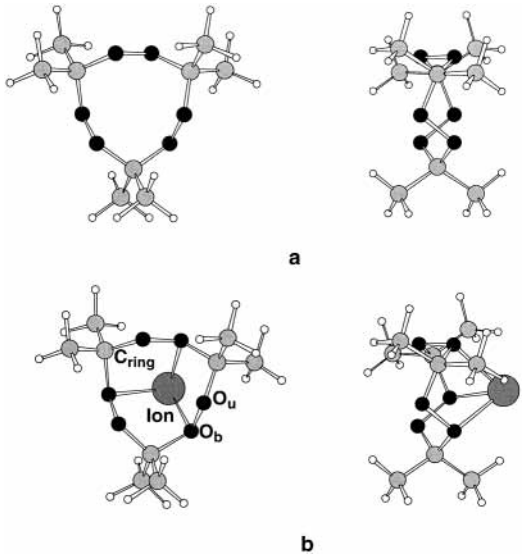

Figure 1. Top view (left) and side view (right) of the lowest-energy geometry for (a) the TATP molecule and (b) the ion−TATP complex (ion = Li^+, Cu^+, Zn^{2+}, Cd^{2+}, In^{3+}).

Results

The binding energies of all complexes investigated are summarized in Table 1. The top and side views of the lowest-energy structures, obtained in the DFT calculations, are shown schematically in Figure 1 for all ions (except Sb^{3+} and Ti^{4+}) and in Figure 2 for the Sb^{3+}−, Sc^{3+}−, and Ti^{4+}−TATP complexes. The ring of the TATP molecule is composed of three carbon atoms, each of which is bound to two methyl groups, and six oxygen atoms in a nonplanar configuration (Figure 1a). Here, O_b and O_u represent oxygen atoms that are bound or unbound, respectively, to the metallic ion. In the case of Li^+, Cu^+, Zn^{2+}, Cd^{2+}, and In^{3+}, the metal ion is positioned in the center of the ring, as seen from the top view, but above (or below) the ring, as seen in the side view (Figure 1b). According to the calculations, when Sb^{3+}, Sc^{3+}, or Ti^{4+} is placed in the center of the TATP ring, cleavage of the three carbon−oxygen bonds and of the TATP ring occurs, and the central ion forms bonds with the three acetone peroxide (AP) molecules (Figure 2).

The binding between the ions and the TATP molecule consists basically of three ion−oxygen bonds that are formed with the

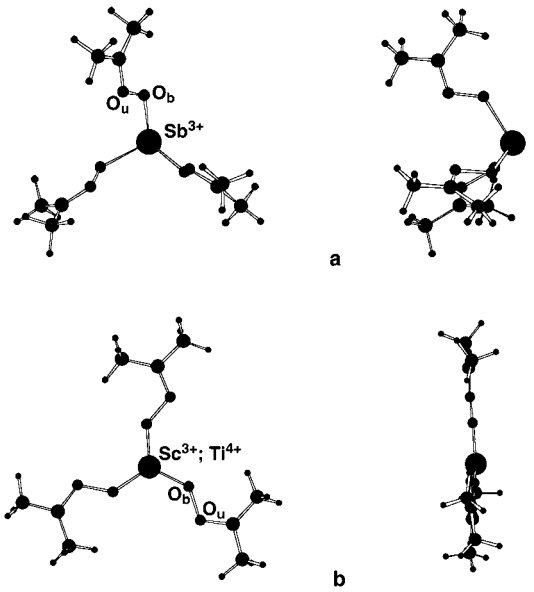

Figure 2. Top view (left) and side view (right) of the lowest-energy geometry for (a) the Sb^{3+}−TATP complex (upper panel) and (b) the Ti^{4+}−TATP complex (lower panel).

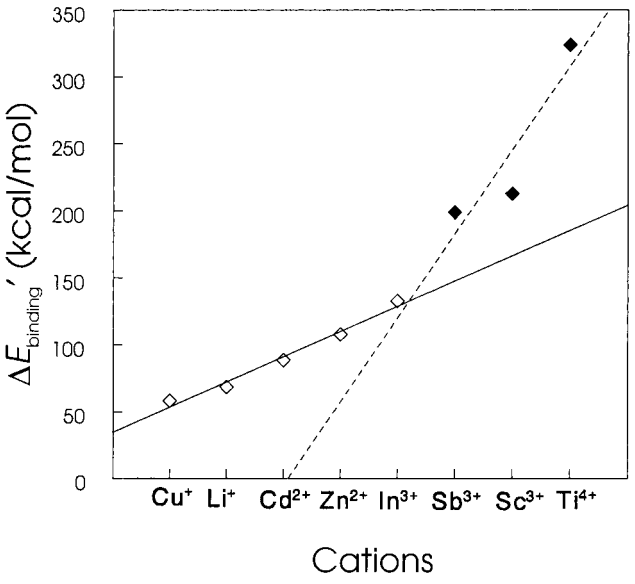

Figure 3. Ion−TATP binding energies obtained at the DFT level were normalized to the ionic radius for the various ions examined. Open diamonds (◊) represent complexes in which TATP is in a closed-ring configuration. Solid diamonds (♦) correspond to the binding of the ion to three AP fragments.

ring oxygen atoms closest to the ion. According to the results obtained in the calculations and summarized in Table 1, the strongest bond is formed between TATP and In^{3+} (in the case of Sb^{3+}, Sc^{3+}, and Ti^{4+}, the bonding is with the TATP fragments). The strength of the ion−TATP bond increases markedly as the charge on the ion increases, where among the divalent ions, zinc forms a stronger bond than does cadmium and between the singly charged ions, Li^+ forms a stronger bond with TATP than does Cu^+. For both singly and doubly charged ions, the ion−TATP bond strength is smaller for the ion with the larger ionic radius. This trend is similar to the trend observed by Glending and Feller[24] in their investigation of the interaction energies between Mg^{2+}, Ca^{2+}, Sc^{2+}, Ba^{2+}, Ra^{2+}, and crown ether (18-crown-6) molecules. In that study, both HF and second-order Moller−Plesset perturbation theory (MP2) were used with the 6-31+G* basis set and Hay and Wadt's relativistic core potential (for the ions). It was clearly demonstrated that the binding energies decrease with increasing ionic radii[24] in agreement with the results obtained in the present study. The binding-energy values reported in ref 24 were in the range of 158−287 kcal/mol at the HF level of calculation and in the range of 167−296 kcal/mol at the MP2 level. These results are in excellent agreement with the DFT results obtained here for the divalent ions Cd^{2+} and Zn^{2+} (Table 1). In addition, the binding energy for Li^+−TATP is also in very good agreement with calculations using a similar level of computations for the Li^+−(18-crown-6) complex.[25]

Thus, the calculated binding energies for ion−TATP complexes for the cases where the molecular ring does not open increase in the order $Cu^+ < Li^+ < Cd^{2+} < Zn^{2+} < In^{3+}$. The binding energy calculated at the B3LYP level and normalized by the ion valence increases in a linear fashion with the same order of the ions as that shown in Figure 3. The ZPE correction at the B3LYP/6-31G** level of theory leads to a small decrease of approximately 2 kcal/mol in the relative energy values. However, this minor modification does not affect the discussion of the trends described above.

In the cases of both Sc^{3+}− and Sb^{3+}−TATP complexes, the HF approach led to a structure that is similar to the one obtained for the other ions investigated, namely, the ion positioned at the center of the TATP molecular ring. The accuracy of the HF results was examined for the Sc^{3+} ion by performing a full-electron calculation. It was found that the TATP remains in a ring shape with the ion attached to the ring center. The binding energy for the Sc^{3+}−TATP complex obtained in the full-electron calculation was 334.44 kcal/mol, which is about 7% smaller than the value obtained using a small basis set (see Table 1). On the other hand, all attempts to obtain a stable structure with a closed molecular ring for Sb^{3+}−, Sc^{3+}−, and Ti^{4+}−TATP complexes at the B3LYP level of theory were not successful. The use of a full-electron basis set for Sc^{3+}, B3LYP/6-31G**, resulted in a bond of 684.50 kcal/mol with a dissociated TATP ring. This bond energy constitutes an approximately 7% increase in binding compared with the data obtained using an effective core potential (ECP) for Sc^{3+} (see Table 1). The geometry optimization in these cases, using the structure obtained for the In^{3+}−TATP complexes as the initial geometry as well as starting from a closed-ring structure calculated at the HF level, reverted to opening of the TATP ring. The calculations performed for the TATP molecules showed that at all levels of calculation the closed-ring structure of TATP is more stable than three acetone peroxide molecules by 5.03 eV (115.94 kcal/mol). The results presented in Table 1, as well as those in Figure 3, show that the stabilization of the Sb^{3+}−, Sc^{3+}−, and Ti^{4+}−TATP complexes relative to the In^{3+}−TATP complex after the molecular ring opens is about 162, 241, and 898 kcal/mol, respectively. Thus, energetically, the opening of the molecular ring is highly advantageous. Moreover, the DFT results also indicate that only a very small energy barrier, or no barrier, separates the two structures of the Sb^{3+}−, Sc^{3+}−, and Ti^{4+}−TATP complexes.

The geometrical changes of the bond distances and angles of the TATP molecule that take place following its interaction with the metallic ions are summarized in Table 2 and graphically presented in Figures 4 and 5. The formation of a complex between TATP and an ion leads to a slight increase in the O_u−O_b bond length. It should be noted that the definitions of O_b and O_u are based on the O−ion separation only. The increases in these bond lengths are about 0.015 Å (see Table 2 and Figure 4). A more pronounced change is observed in the C_{ring}−O_b equilibrium distance that increases from 0.035 to 0.115 Å upon

TABLE 2: Some Distances (Å) and Angles (deg) in the TATP Molecule, Ion−TATP Complexes, the Acetone Peroxide (AP) Molecule, and Ion−$(AP)_3$ Complexes Calculated at the B3LYP/6-31G+CRENBL ECP Level of the Theory**

		ion−TATP						ion−$(AP)_3$		
	TATP	Cu^+	Li^+	Cd^{2+}	Zn^{2+}	In^{3+}	AP	Sb^{3+}	Sc^{3+}	Ti^{4+}
ionic radii		0.96	0.68	0.97	0.74	0.81		0.76	0.81	0.68
$C_{ring}-O_b$	1.420	1.455	1.455	1.487	1.521	1.535	2.262	2.287	2.301	2.360
$C_{ring}-O_u$	1.420	1.419	1.419	1.417	1.415	1.418	1.276	1.296	1.295	1.320
O_b-O_u	1.462	1.477	1.477	1.475	1.493	1.475	1.371	1.450	1.434	1.460
ion−O_b		2.153	1.950	2.294	1.977	2.245		2.068	1.952	1.797
ion−O_b[a]		2.278	1.971	2.290	1.983	2.149		2.110	2.072	1.772
ion−O_u		2.937	2.744	3.103	2.731	3.245		3.125	3.006	2.952
ion−O_u[a]		3.116	2.764	3.125	2.890	2.964		2.970	2.944	2.892
$O_u-C_{ring}-O_b$	113.20	110.82	110.02	109.52	107.80	109.95				
O_b−ion−O_b		80.06	88.40	76.09	90.10	78.43		104.04	119.95	117.86

[a] The distances were calculated at the HF/6-31G**+CRENBL ECP level of the theory. (The structures of Sb^{3+}−TATP and Sc^{3+}−TATP as calculated at HF/6-31G** include a closed TATP ring, but in Ti^{4+}−TATP at the HF level, the molecular ring is already open.)

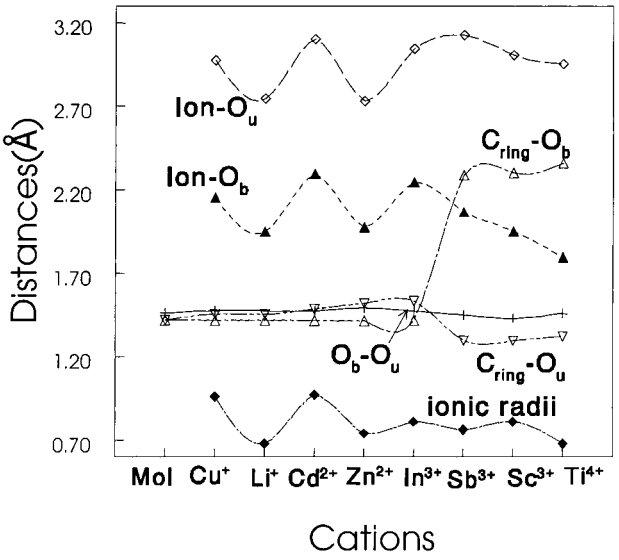

Figure 4. The change in interatomic distances as a function of the identity of the ion examined. Also shown, at the bottom, are the ionic radii of the different ions used in the study.

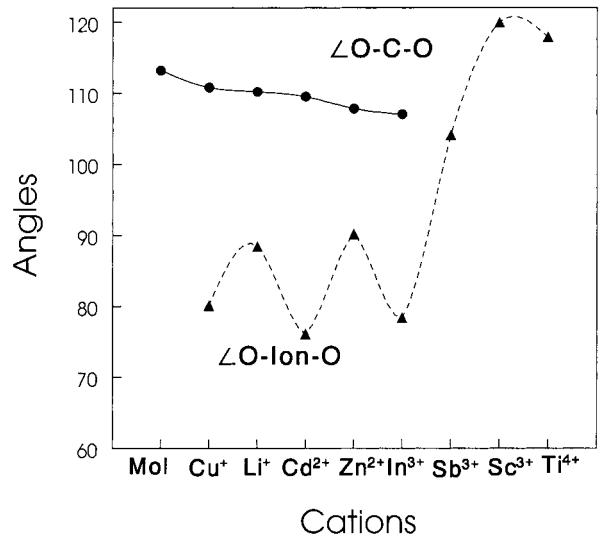

Figure 5. Change in O−C−O and O−ion−O angles as a function of the identity of the ion.

changing the central ion from Cu^+ to In^{3+}, respectively. Here, C_{ring} represent the carbon atom in the TATP ring. For all of the systems examined, the $C_{ring}-O_u$ distances are nearly constant. The variations in the $C_{ring}-O_b$ distances in the complex suggests that these bonds are weaker than those in the bare TATP molecule.

The ion−O distances obtained from the DFT as well as the HF calculations are shown in Table 2. It was found that the two computational methods yield very similar ion−O distances. The ion−O_b and ion−O_u distances vary considerably when the central ion is changed. The ion−O_b distances in the different ion−TATP complexes span the range of 1.9−2.3 Å. This range is similar to that of the ion−O distances in the case of crown ethers.[23] The ion−O_u distances in the ion−TATP complexes are much longer, spanning the range of 2.7−3.25 Å. It should be noted that the length of both ion−O_u and ion−O_b correlate directly with the ionic radius of the central ions[26] (see Table 2 and Figure 4). Furthermore, the O_u−ion−O_b angles change in a more pronounced fashion than do other angles in the ion−TATP complex. The variation in the O_u−ion−O_b angles for different ions exhibits an inverse correlation with the ionic radii (see Table 2 and Figure 5). It is interesting to note that the $O_u-C_{ring}-O_b$ angle seems to correlate with the binding energy of the complex; the angle increases for larger binding energy. This discussion of the geometrical changes in the ion−TATP complex apply only to systems in which the TATP ring does not open. In the case of the three ions that form ion−$(AP)_3$ molecules, a much larger decrease in the $C_{ring}-O_u$ distances are observed (see Table 2 and Figure 4). This decrease is associated with the $C_{ring}-O_u$ bond becoming practically a double bond.

The electronic charge distributions in the TATP molecule and the ion−TATP complexes, as obtained by the Mulliken and NBO population analysis on individual atoms and groups of atoms, are shown in Table 3. The negative charge on the O_b atoms in the ion−TATP complex is somewhat larger than that in the TATP molecule. On the other hand, a decreased charge on O_u is observed following the ion−TATP complex formation. More pronounced changes are observed in the magnitude of the charges on methyl groups and the ions. It is quite clear that in all cases a large fraction of the ion's positive charge is redistributed almost evenly among the methyl groups. Comparison of the ion−TATP binding and the amount of charge transfer in the complex exhibits a positive correlation, namely, larger charge transfer corresponds to stronger binding energy. This correlation suggests that bond formation in the ion−TATP complex includes a large contribution from Coulomb interactions.

As discussed above, Sb^{3+}−, Sc^{3+}−, and Ti^{4+}−TATP complexes simulated at the B3LYP level exhibit a minimum-energy structure with opening of the TATP ring. Thus, the ion−TATP structure for these systems corresponds to an ion bound to three

TABLE 3: Charges of Atoms and Groups in the TATP Molecule, Ion−TATP Complexes, the Acetone Peroxide (AP) Molecule, and Ion−$(AP)_3$ Complexes Calculated at the B3LYP/6-31G+CRENBL ECP Level of the Theory**

		complex ion−TATP						ion−$(AP)_3$		
	TATP	Cu^+	Li^+	Cd^{2+}	Zn^{2+}	In^{3+}	AP	Sb^{3+}	Sc^{3+}	Ti^{4+}
					Mulliken Scheme					
O_b	−0.31	−0.38	−0.35	−0.32	−0.45	−0.34	−0.39	−0.45	−0.47	−0.38
O_u	−0.31	−0.28	−0.25	−0.22	−0.20	−0.17	−0.14	−0.15	−0.12	−0.12
C_{ring}	0.54	0.48	0.48	0.46	0.40	0.41	0.40	0.46	0.46	0.48
C_{met1}	0.04	0.11	0.13	0.19	0.21	0.29	0.05	0.28	0.28	0.36
C_{met2}	0.04	0.14	0.14	0.23	0.24	0.33	0.08	0.30	0.28	0.38
ion		0.74	0.52	1.02	1.39	1.44		1.68	1.69	1.82
					NBO Scheme					
O_b	−0.33	−0.39	−0.41	−0.41	−0.45	−0.39	−0.45	−0.61	−0.56	−0.41
O_u	−0.33	−0.29	−0.28	−0.25	−0.24	−0.20	−0.14	−0.16	−0.16	−0.13
C_{ring}	0.58	0.57	0.56	0.56	0.56	0.55	0.52	0.69	0.70	0.71
C_{met1}	0.04	0.06	0.06	0.10	0.11	0.17	0.03	0.18	0.16	0.23
C_{met2}	0.04	0.10	0.10	0.14	0.16	0.22	0.04	0.19	0.20	0.28
ion		0.87	0.92	1.58	1.61	1.94		2.14	2.04	1.98

AP molecules, as shown in Figure 2. In the following section, we shall try to shed some light on the reasons for the opening of the TATP ring. The antimony atom has an electronic configuration of $[Kr]4d^{10}5s^25p^3$, and the the Sb^{3+} ion has a $[Kr]4d^{10}5s^2$ electronic configuration. The electronic structures of scandium and titanium atoms are $[Ar]3d^14s^2$ and $[Ar]3d^24s^2$, respectively, and that of Sc^{3+} and Ti^{4+} is the closed-shell structure of [Ar]. The other ions examined in this study, Li^+, Cu^+, Zn^{2+}, Cd^{2+}, and In^{3+}, also have closed-shell electronic structures. Hence, it is unlikely that the TATP ring opening is due to differences in the electronic structure of the ions. Let us examine the nature of the vacant orbitals on the various ions. The three vacant orbitals on Sb^{3+} are p type, those on Sc^{3+} and Ti^{4+} are d and s type, respectively, on In^{3+}, s and p type, and for the other ions, only s orbitals become vacant. To form a bond between an ion and the TATP molecule, when the ion gets close to the molecule, it is expected that the vacant orbitals of the ion will interact with the p orbitals on the three O_b's. Thus, it is expected that the diffuse nature of the vacant orbitals on the ion and their symmetry will play an important role in the bond formation between TATP and the ion. We have carefully examined all the occupied molecular orbitals (MO) of the ion−TATP complexes. The contribution to the binding from ion orbitals was found only for ions that have vacant p or d orbitals (in their ionic form). An example of such a MO for the case of the Sb^{3+}−TATP complex is shown in Figure 6. Clearly, the MOs correspond to three bonds formed between the ion and the AP molecules. Similar bonding MOs were also found for the Sc^{3+}− and Ti^{4+}−TATP complexes. For In^{3+}, which has only one vacant p orbital (as an ion), we found a MO that showed a small contribution from the 5p orbital on the metal. However, this contribution was not substantial enough to induce the rupture of the TATP ring and the formation of three bonds to AP molecules, as in the case of Sb, Sc, and Ti. To support the discussion above, we performed a NBO analysis[23] of the ions in the complex as obtained in the B3LYP calculation. The results are presented in Table 4 as natural orbital populations of orbitals on the ions in the complexes. It is clear from these results that when the TATP ring does not open the ions do not possess appreciable populations in their p and d orbitals (which are empty for isolated ions). On the other hand, when three bonds to the AP are formed, the ions exhibit appreciable populations in their previously empty p and d orbitals (e.g., the Sb^{3+}, Sc^{3+}, and Ti^{4+}). In the case of In^{3+}, we find a small electron population in the 5p orbital, but it is not enough for the formation of three bonds to the AP fragments.

The nature of the vacant orbitals on the ion is also manifested in the structure of the resultant ion−$(AP)_3$ molecule that is formed. As can be seen in Figure 2, the Sb^{3+}−$(AP)_3$ molecule is not planar, but for Sc^{3+} and Ti^{4+}, a planar molecule is obtained. This difference in the molecular structure is a direct manifestation of the symmetry of the vacant orbitals on the ions. For all other ions, the vacant orbitals are of s type, and they

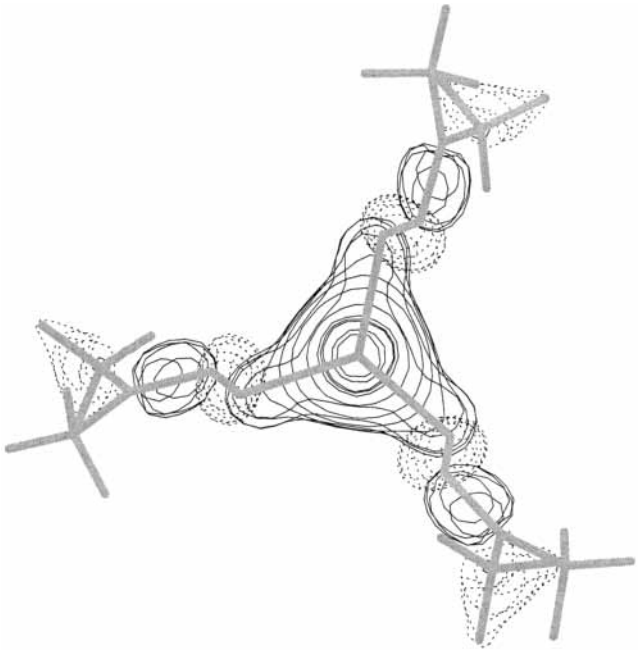

Figure 6. Electronic charge density distribution of one occupied molecular orbital in the Sb^{3+}−TATP complex. The binding to the three AP molecules formed following ring opening is clearly seen.

TABLE 4: Natural Bond Orbital (NBO) Populations Shown as Electron Configurations for the Ions in the Different Complexes[a]

ion	molecular form	electron configuration
Cu^+	TATP	[core]2s(0.14)3d(9.97)5s(0.01)
Li^+	TATP	[core]2s(0.03)2p(0.01)
Cd^{2+}	TATP	[core]5s(0.38)4d(9.99)5p(0.04)
Zn^{2+}	TATP	[core]3s(0.38)3d(9.99)4p(0.01)4d(0.01)
In^{3+}	TATP	[core]5s(0.83)**5p(0.20)**5d(0.01)6p(0.01)
Sb^{3+}	$(AP)_3$	[core]5s(1.81)**5p(1.02)**5d(0.02)6p(0.01)
Sc^{3+}	$(AP)_3$	[core]4s(0.08)**3d(0.87)**4p(0.01)4d(0.02)
Ti^{4+}	$(AP)_3$	[core]4s(0.08)**3d(1.93)**4p(0.01)4d(0.02)

[a] The analysis was performed using the results of the B3LYP calculations. The NBO calculations were performed with the NBO 3.1 program as implemented in Gaussian 98.[23] Bold symbols correspond to orbitals that may induce dissociation of the TATP ring.

were not found to contribute to any of the occupied molecular orbitals in the complex. Therefore, for these systems, the main contribution to the ion−TATP interaction is due to the charge transfer, that is, it is electrostatic in nature.

Summary

The results of the calculations presented above yield a detailed picture of the structure and conformation of a free TATP molecule and of seven TATP−ion complexes. It must be emphasized that the conformational information is based on theoretical considerations of gas-phase single-molecule complexes. The difficulties in actually producing layers of ions on an active surface of a solid-state device were not examined or discussed in the present work. Thus, these results may serve as guidelines for experimentalists who are trying to develop sensitive, specific sensors for the detection of TATP. The fact that TATP may undergo partial dissociation to diacetone diperoxide (DADP) should not affect the detector as long as some TATP is present.

Among all the ions studied, the largest binding energy was found between TATP molecules and In^{3+} ions. According to the calculations, the complexes of TATP with Sb^{3+} and Ti^{4+} lead to the opening of the TATP ring and dissociation of TATP into three acetone peroxide molecules attached to the ion. Of the divalent ions, the TATP−Zn^{2+} complex was energetically favored over the TATP−Cd^{2+} complex by more than 23 kcal/mol. Among the two monovalent ions, the complex with Li^{+} was favored over the complex with Cu^{+}. Once the ion radius is taken into account, the binding energy corresponds to the radius of the central ion, thus the smaller ion has a larger binding energy. Geometric changes in the TATP ring follow the same trend.

Acknowledgment. This study was supported by the Israel Atomic Energy Commission and the Israel Council for Higher Education.

References and Notes

(1) Muller, D.; Abramovich-Bar, S.; Shelef, R.; Tamiri, T.; Sonenfeld, D.; Levy, A. The post-explosion analysis of TATP. Fourth Conference of Isreal Society of Analytical Chemists, Tel-Aviv, Israel, January 24−25, 2001.

(2) White, G. M. *J. Forensic Sci.* **1992**, *37*, 652−656.

(3) Middle-class woman planted an embassy bomb, *The Independent*, London, Oct 8, 1996.

(4) *Containing the Threat from Illegal Bombings: An Integrated National Strategy for Marking, Tagging, Rendering Inert and Licensing Explosives and Their Precursors*, Commission on Physical Science, Mathematics and Applications, National Academy Press: 1998.

(5) Wolffelstil, R. *Der. Deut. Chem. Ges.* **1895**, *28*, 2265.

(6) Zitrin, S.; Kraus, S.; Glattenstein, B. Identification of Two Rare Explosives, Proceedings of the International Symposium on the Detection of Explosives, Quantico, VA, 1983; pp 137−141.

(7) (a) Milas, N. A.; Golubovic, N. *J. Am. Chem. Soc.* **1959**, *81*, 6459. (b) Evans, H. E.; Tulleners, F. A. J.; Sanchez, B. L.; Rasmussen, C. A. *J. Forensic Sci.* **1986**, *31*, 1119−1125.

(8) Chladek, J. The Identification of Organic Peroxides. In Advanced Analytical Detection of Explosives, Proceedings of the Fourth International Symposium of the Analytical Detection of Explosives, Yinon, J., Ed.; Kluwer Academic Publishers: Dordrecht, The Netherlands, 1993; pp 73−76.

(9) Bellamy, A. J. *J. Forensic Sci.* **1999**, *44*, 603−608.

(10) Kirk-Othmer Encyclopedia of Chemical Technology, Grayson, M., Ed.; Wiley & Sons: New York, 1977.

(11) Harsanyi, G. *Sens. Rev.* **2000**, *20*, 98−105.

(12) Reyzer, M. L.; Brodbelt, J. S.; Marchand, A. P.; Chen, Z.; Huang, Z.; Namboothiri, I. N. N. *Int. J. Mass Spectrom.* **2001**, *204*, 133−142.

(13) (a) Dunning, T. H., Jr.; Hay, P. J. In *Methods of Electronic Structure Theory*; Schaefer, H. F., III, Ed.; Plenum Press: New York, 1977; p 2. (b) Hay, P. J.; Wadt, W. R. *J. Chem. Phys.* **1985**, *82*, 284−298.

(14) Hurley, M. M.; Pacios, L. F.; Christiansen, P. A.; Ross, R. B.; Ermler, W. C. *J. Chem. Phys.* **1986**, *84*, 6840−6852.

(15) LaJohn, L. A.; Christiansen, P. A.; Ross, R. B.; Atashroo, T.; Ermler, W. C. *J. Chem. Phys.* **1987**, *87*, 2812−2824.

(16) Becke, A. D. *J. Chem. Phys.* **1993**, *98*, 5648−5652.

(17) Lee, C.; Yang, W.; Parr, R. G. *Phys. Rev. B: Condens. Matter* **1988**, *37*, 785−789.

(18) Luna, A.; Amekraz, B.; Tortajada, J. *J. Phys. Chem. B* **2000**, *104*, 110−118.

(19) Hoyau, S.; Ohanessian, G. *Chem. Phys. Lett.* **1997**, *280*, 266−272.

(20) Bauschlicher, C.; Ricca, A.; Partrige, H.; Langhoff, S. R. *Recent Advances in Density Functional Theory*; Chong, D. P., Ed.; Word Scientific Publishing Co.: Singapore, 1997; part II.

(21) Frisch, M. J.; Trucks, G. W.; Schlegel, H. B.; Scuseria, G. E.; Robb, M. A.; Cheeseman, J. R.; Zakrzewski, V. G.; Montgomery, J. A., Jr.; Stratmann, R. E.; Burant, J. C.; Dapprich, S.; Millam, J. M.; Daniels, A. D.; Kudin, K. N.; Strain, M. C.; Farkas, O.; Tomasi, J.; Barone, V.; Cossi, M.; Cammi, R.; Mennucci, B.; Pomelli, C.; Adamo, C.; Clifford, S.; Ochterski, J.; Petersson, G. A.; Ayala, P. Y.; Cui, Q.; Morokuma, K.; Malick, D. K.; Rabuck, A. D.; Raghavachari, K.; Foresman, J. B.; Cioslowski, J.; Ortiz, J. V.; Stefanov, B. B.; Liu, G.; Liashenko, A.; Piskorz, P.; Komaromi, I.; Gomperts, R.; Martin, R. L.; Fox, D. J.; Keith, T.; Al-Laham, M. A.; Peng, C. Y.; Nanayakkara, A.; Gonzalez, C.; Challacombe, M.; Gill, P. M. W.; Johnson, B. G.; Chen, W.; Wong, M. W.; Andres, J. L.; Head-Gordon, M.; Replogle, E. S.; Pople, J. A. *Gaussian 98*, revision A.7; Gaussian, Inc.: Pittsburgh, PA, 1998.

(22) Mulliken, R. S. *J. Chem. Phys.* **1955**, *23*, 1833−1840. Mulliken, R. S. *J. Chem. Phys.* **1955**, *23*, 1841−1846. Mulliken, R. S. *J. Chem. Phys.* **1962**, *36*, 3428−3439.

(23) (a) Foster, J. P.; Weinhold, F. *J. Am. Chem. Soc.* **1980**, *102*, 7211. (b) Reed, A. E.; Weinstoc, R. B.; Weinhold, F. *J. Chem. Phys.* **1985**, *83*, 735. (c) Reed, A. E.; Curtiss, L. A.; Weinhold, F. *Chem. Rev.* **1988**, *88*, 899.

(24) Glendening, E. D.; Feller, D. *J. Am. Chem. Soc.* **1996**, *118*, 6052−6059.

(25) Glendening, E. D.; Feller, D.; Thompson, M. A. *J. Am. Chem. Soc.* **1994**, *116*, 10657−10669.

(26) WebElements periodic table. www.webelements.com.